Journal of Biomechanics 47 (2014) 3201–3209

Contents lists available at ScienceDirect

Journal of Biomechanics

journal homepage: www.elsevier.com/locate/jbiomech
www.JBiomech.com

Continuum description of the Poisson's ratio of ligament and tendon under finite deformation

Aaron M. Swedberg [a,b,c], Shawn P. Reese [a,b,c], Steve A. Maas [a,b,c], Benjamin J. Ellis [a,b,c], Jeffrey A. Weiss [a,b,c,*]

[a] Department of Bioengineering, The University of Utah, 36 South Wasatch Drive, Room 3100, Salt Lake City, UT 84112, USA
[b] Department of Orthopedics, The University of Utah, 36 South Wasatch Drive, Room 3100, Salt Lake City, UT 84112, USA
[c] Scientific Computing and Imaging Institute, The University of Utah, 36 South Wasatch Drive, Room 3100, Salt Lake City, UT 84112, USA

ARTICLE INFO

Article history:
Accepted 18 May 2014

Keywords:
Ligament
Poisson's ratio
Soft tissue mechanics

ABSTRACT

Ligaments and tendons undergo volume loss when stretched along the primary fiber axis, which is evident by the large, strain-dependent Poisson's ratios measured during quasi-static tensile tests. Continuum constitutive models that have been used to describe ligament material behavior generally assume incompressibility, which does not reflect the volumetric material behavior seen experimentally. We developed a strain energy equation that describes large, strain dependent Poisson's ratios and nonlinear, transversely isotropic behavior using a novel method to numerically enforce the desired volumetric behavior. The Cauchy stress and spatial elasticity tensors for this strain energy equation were derived and implemented in the FEBio finite element software (www.febio.org). As part of this objective, we derived the Cauchy stress and spatial elasticity tensors for a compressible transversely isotropic material, which to our knowledge have not appeared previously in the literature. Elastic simulations demonstrated that the model predicted the nonlinear, upwardly concave uniaxial stress–strain behavior while also predicting a strain-dependent Poisson's ratio. Biphasic simulations of stress relaxation predicted a large outward fluid flux and substantial relaxation of the peak stress. Thus, the results of this study demonstrate that the viscoelastic behavior of ligaments and tendons can be predicted by modeling fluid movement when combined with a large Poisson's ratio. Further, the constitutive framework provides the means for accurate simulations of ligament volumetric material behavior without the need to resort to micromechanical or homogenization methods, thus facilitating its use in large scale, whole joint models.

1. Introduction

When fibrous connective tissues such as ligaments and tendons are stretched under quasi-static uniaxial extension along the fiber direction, they exhibit large Poisson's ratios (Hewitt et al., 2001; Lynch et al., 2003; Screen and Cheng, 2007). Reported values range from 0.8 ± 0.3 for rat tail tendon fascicles (Screen and Cheng, 2007) to 2.98 ± 2.59 for bovine flexor tendons (Lynch et al., 2003). Large Poisson's ratios have also been observed in other biological materials, including collagen gels (Reese et al., 2013) and fibrin polymer networks (Purohit et al., 2011). These Poisson's ratios indicate volume loss in the tissue during tensile loading (Reese et al., 2010). Since tendons and ligaments are composed of 65–75% water by weight (Benjamin and Ralphs, 1997), volume loss under tensile loading suggests exudation of fluid from the ligament, as has been reported experimentally (Hannafin and Arnoczky, 1994; Lanir et al., 1988; Wellen et al., 2004). It has been proposed that fluid movement under tensile loading is one of the primary mechanisms by which fibroblasts in the ligament receive and exchange nutrients (Butler et al., 1997; Chen et al., 1998; Lavagnino et al., 2008; Urschel et al., 1988)

Using a micromechanical finite element (FE) model, we previously demonstrated that the characteristic nonlinear stress–strain behavior and large Poisson's ratios for ligament and tendon can be predicted by modeling a helical arrangement of fibrils within a crimped fiber (Reese et al., 2010). Micromechanical models are computationally expensive and thus are not suited for large scale computation for modeling entire joints such as the knee. Continuum models are considerably more computationally economical for FE simulations, but none of the three-dimensional constitutive models that have been applied to ligament and tendon mechanics to date can describe the large Poisson's ratios

* Correspondence to: Department of Bioengineering, University of Utah, 50 S. Central Campus Drive, Rm. 2480, Salt Lake City, UT 84112, USA.
Tel.: +801 634 5442; fax: +801 585 5361.
E-mail address: jeff.weiss@utah.edu (J.A. Weiss).

http://dx.doi.org/10.1016/j.jbiomech.2014.05.011
0021-9290/

seen experimentally. Constitutive models that have been used previously to represent ligaments and tendons in FE simulations generally assume incompressibility (e.g., Hirokawa and Tsuruno, 2000; Pioletti et al., 1998; Song et al., 2004; Weiss and Gardiner, 2001). For a transversely isotropic material loaded in tension along its fiber direction, this implies a Poisson's ratio of 0.5. This does not accurately reflect experimentally observed ligament and tendon volumetric behavior during quasi-static testing.

The objective of this research was to develop a continuum based hyperelastic constitutive model that can describe both the stress–strain relationship of tendons and ligaments under tensile loading, as well as the large, strain dependent Poisson's ratios observed experimentally. This constitutive model was implemented in the open source, nonlinear finite element solver FEBio (Maas et al., 2012). We hypothesized that during biphasic simulations, accurate description of the large Poisson's ratio in the constitutive model for the solid phase would predict large outward fluid flux and substantial stress-relaxation, suggesting that the viscoelastic behavior of ligaments can be predicted by modeling fluid movement when combined with a large Poisson's ratio.

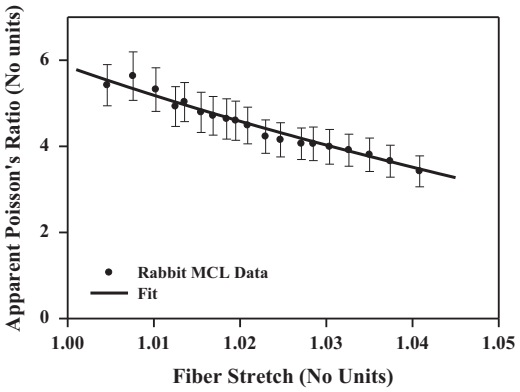

Fig. 1. The experimentally measured apparent Poisson's ratio as a function of fiber stretch from measurements of fiber and transverse strain in mature rabbit medial collateral ligament (MCL) under uniaxial extension ($N=6$) (Weiss et al., 1992). The data was fit to Eq. (15), represented by the solid line. The equation fit the data with an R^2 value of 0.967 when the parameters m and ν_0 were selected to be -100 and 5.85, respectively.

2. Materials and methods

2.1. Constitutive model

To describe volumetric behavior of ligament and tendon, we developed a strain energy that could describe the volume loss in ligaments due to transverse retraction during uniaxial extension. Consider uniaxial extension of a transversely isotropic material along the fiber direction, with fibers oriented along the x-axis. The incremental deformation of the material along the transverse y direction, dy, is related to incremental deformation in the fiber x direction, dx, via the Poisson's ratio, ν:

$$\frac{dy}{y} = -\nu\frac{dx}{x} \tag{1}$$

If ν is assumed to be a general function of the deformation, then it is sometimes referred to as the Poisson's function (Beatty and Stalnaker, 1986). We will use these terms interchangeably. If the Poisson's ratio depends on stretch along the x-direction and we consider a specific increment in deformation, integration of the above equation yields:

$$\int_{y_0}^{y_0+\Delta y}\frac{dy}{y} = -\int_{x_0}^{x_0+\Delta x}\nu(x)\frac{dx}{x} \tag{2}$$

The variables y_0 and x_0 are reference lengths along the y and x directions, respectively, and Δy and Δx are changes in overall length described by the deformation. The equation can be expressed in terms of the fiber stretch ratio λ and the transverse stretch ratio α by making the equivalences:

$$y = y_0\alpha, \quad x = x_0\lambda, \quad dy = y_0 d\alpha, \quad dx = x_0 d\lambda. \tag{3}$$

Substituting these values into Eq. (2), the differential equation can be written as:

$$\int_1^{\alpha^*}\frac{d\alpha}{\alpha} = -\int_1^{\lambda^*}\nu(\lambda)\frac{d\lambda}{\lambda} \tag{4}$$

The variables λ^* and α^* are specific fiber and transverse stretch ratios resulting from the deformation.

We calculated the Poisson's ratio from previous measurements of fiber and transverse strain in mature rabbit medial collateral ligament (MCL) under uniaxial extension ($N=6$) (Weiss et al., 1992) (Fig. 1). Based on these data, Poisson's ratio was represented as a linear function of fiber stretch, λ:

$$\nu(\lambda) = m(\lambda-1)+\nu_0 \tag{5}$$

Here m and ν_0 are the slope and y intercept of the function, respectively. Substituting this expression into Eq. (4) yields the equation:

$$\int_1^{\alpha^*}\frac{d\alpha}{\alpha} = -\int_1^{\lambda^*}(m(\lambda-1)+\nu_0)\frac{d\lambda}{\lambda} \tag{6}$$

Integration of both sides of the equation by separation of variables yields an expression for the transverse stretch α in terms of the fiber stretch λ and the parameters of the function describing the Poisson's ratio that is valid for finite deformation:

$$\alpha^* = \lambda^{*m-\nu_0}e^{-m(\lambda^*-1)} \tag{7}$$

Since λ^* and α^* are the actual stretch ratios of interest, we drop the asterisks and refer to them as λ and α hereafter. This new definition can be used to derive a strain energy term describing the volumetric deformation of a material. For a representative element of a transversely isotropic material stretched homogeneously along the fiber direction by λ, the change in the cross sectional area in the transverse plane is related to the transverse fiber stretch:

$$\frac{da}{dA} = \alpha^2 = \lambda^{2(m-\nu_0)}e^{-2m(\lambda-1)} \tag{8}$$

where dA and da represent the incremental cross sectional area of the material normal to the direction of loading in the undeformed and deformed configurations, respectively. Squaring both sides yields the equation:

$$\left(\frac{da}{dA}\right)^2 = \lambda^{4(m-\nu_0)}e^{-4m(\lambda-1)} \tag{9}$$

An alternative equation relating the squared area ratio in Eq. (9) to the invariants of a transversely isotropic material was derived by using Nanson's relation and the Cayley–Hamilton theorem (Appendix A):

$$\left(\frac{da}{dA}\right)^2 = I_5 - I_1I_4 + I_2 \tag{10}$$

The variables I_1–I_5 are four of the five strain invariants for a transversely isotropic material:

$$I_1 = \mathrm{tr}(\mathbf{C}), \quad I_2 = \tfrac{1}{2}((\mathrm{tr}(\mathbf{C}))^2 - \mathrm{tr}(\mathbf{C}^2)), \quad I_4 = \mathbf{a}_0\cdot\mathbf{C}\cdot\mathbf{a}_0 = \lambda^2, \quad I_5 = \mathbf{a}_0\cdot\mathbf{C}^2\cdot\mathbf{a}_0 \tag{11}$$

Here, $\mathbf{C}$ is the right Cauchy-Green deformation tensor, $\mathbf{C}=\mathbf{F}^T\mathbf{F}$, where $\mathbf{F}$ is the deformation gradient tensor and $\mathbf{a}_0$ is a unit vector defining the initial preferred direction. To our knowledge, the relationship in Eq. (10) has not been presented previously in the literature.

If the deformation of the material is compatible with the deformation prescribed by the parameters of the Poisson's ratio, Eqs. (9) and (10) should be equal to each other. Thus, their ratio should be equal to 1.0. A logarithmic form of a strain energy equation was designed to enforce this constraint:

$$W_{vol} = \frac{\kappa}{2}\left(\ln\left(\frac{I_5 - I_1I_4 + I_2}{I_4^{2(m-\nu_0)}e^{-4m(\lambda-1)}}\right)\right)^2 \tag{12}$$

Here, κ is a penalty parameter used to enforce the constraint represented by the parameters for the Poisson's ratio. The logarithmic form is a common choice for a penalty function (Weiss et al., 2002). It ensures that the strain energy of the function is minimized when the deformation experienced by the material as described by the numerator is equal to the deformation prescribed by the parameters for the Poisson's function in the denominator. When this occurs, the ratio between the numerator and denominator is equal to one and the natural logarithm is zero. Any discrepancy between the numerator and the denominator will thus cause the strain energy to be non-zero. Increasing the value of κ will amplify the effect of any discrepancy, further increasing the strain energy away from its minimum value. Note also that $W_{vol}=0$ in the reference configuration and is strictly positive (see Supplementary File A for further investigation of the behavior of W_{vol}).

To test this volumetric term, we combined it with an exponential transversely isotropic fiber strain energy representing the behavior of the collagen fibers (Guerin and Elliott, 2007; Quapp and Weiss, 1998) and a compressible neo-Hookean strain energy representing the isotropic behavior of the extrafibrillar

matrix (Bonet and Wood, 1997):

$$W = W_{fiber} + W_{matrix} + W_{vol},$$

$$W_{fiber} = \frac{1}{2}\frac{c_1}{c_2}(e^{c_2(\lambda-1)^2}-1),$$

$$W_{matrix} = \frac{\mu}{2}(I_1-3) - \mu\ln(\sqrt{I_3}). \quad (13)$$

To implement this constitutive model, we derived the Cauchy stress and spatial elasticity tensors for a general compressible, transversely isotropic hyperelastic material (Appendix B). To our knowledge, these equations have not appeared in the literature previously. These equations were then specialized for the strain energy in Eq. (13), and the constitutive model was implemented in the FEBio finite element software (Maas et al., 2012).

The apparent Poisson's ratio ν_{app}, is the traditional small strain definition of Poisson's ratio calculated using the engineering strain and equivalently be defined in terms of the fiber and transverse stretch ratios:

$$\nu_{app} = -\frac{\alpha-1}{\lambda-1} \quad (14)$$

By substituting our expression for α in Eq. (7) into Eq. (14), we obtain an expression for the apparent Poisson's ratio of our model:

$$\nu_{app} = -\frac{\lambda^{m-\nu_0}e^{-m(\lambda-1)}-1}{\lambda-1} \quad (15)$$

Note that the linear function chosen to describe the Poisson's ratio in Eq. (5) described the instantaneous true strain definition of the Poisson's ratio, while the apparent Poisson's ratio described in Eq. (15) is based on the engineering strain as measured from the reference configuration and is consequently nonlinear. Defining this apparent Poisson's ratio allows us to compare our model to experimentally measured Poisson's ratio data, which typically uses the engineering strain definition shown above.

The parameters m and ν_0 were chosen by fitting equation Eq. (15) to the data in Fig. 1. This equation fit the rabbit MCL data with $R^2=0.967$ when $m=-100$ and $\nu_0=85$. The parameters c_1, c_2, and μ were found by fitting the stress–strain behavior along the fiber direction to experimental data for human MCL stretched along the fiber direction (Quapp and Weiss, 1998) (Table 1). The initial penalty parameter κ was selected so that the uniaxial Poisson's ratio was within 0.5% of its predicted value as calculated at 3% fiber strain.

2.2. Quasi-static simulation of uniaxial extension

A single-element simulation of a uniaxial tensile test was used to verify implementation of the constitutive model in FEBio. Since uniaxial extension of this elastic material along the fiber direction produces a homogeneous deformation, an analytical solution for the Cauchy stress was derived from the strain energy derivatives using Mathematica (Wolfram Research, Champaign, IL) (Appendix C). This analytical solution allowed the verification of the FE implementation in FEBio. The Cauchy stress for uniaxial tension along the fiber direction was calculated using an iterative procedure that determined the transverse stretch α that constrained the transverse stress to zero. For the FE simulation, prescribed displacements were applied to extend model along the fiber direction to 6% uniaxial strain, and the resulting stress and apparent Poisson's ratio were obtained for the FE solution using the new constitutive model. Boundary conditions were prescribed based on the one-element model representing a 1/8th symmetry model. The simulation was repeated with a nearly incompressible constitutive model for ligament behavior, consisting of a transversely isotropic exponential fiber strain energy term and an isotropic Mooney–Rivlin term for the matrix (Quapp and Weiss, 1998). The material coefficients for the nearly incompressible model were taken from a published study (Quapp and Weiss, 1998).

Table 1
Values for the parameters in the strain energy function as defined in Eqs. (12) and (13).

Parameter	Value
c_1 (MPa)	90
c_2	160
μ (MPa)	0.025
κ (MPa)	1.55
m	−100
ν_0	5.85

2.3. Biphasic simulation of uniaxial stress relaxation

A biphasic FE simulation of uniaxial stress relaxation was performed to assess the ability of the new constitutive model to describe the time-dependent material behavior of ligament and tendon. The permeability of the material was described by a strain-dependent isotropic Holmes–Mow constitutive model (Holmes and Mow, 1990), fit to published experimental data for transverse permeability of MCL (Weiss and Maakestad, 2006). The solid phase was represented by the new constitutive model and a quarter-symmetry mesh was constructed to represent a ligament with a cylindrical cross-section, having a radius of 1 mm. The fiber direction was oriented along the long axis of the cylinder (Fig. 2). The radius was chosen to replicate the approximate cross sectional area of the samples reported in a previous study that examined the viscoelastic material behavior of human MCL (Bonifasi-Lista et al., 2005). A preliminary stress-relaxation simulation was conducted to select the penalty parameter κ, mimicking the applied displacement protocol of the longitudinal stress relaxation experiment in Bonifasi-Lista et al. (Bonifasi-Lista et al., 2005). The reaction force along the fiber direction was used to quantify the time-dependent behavior of the model. The penalty parameter κ was altered until the relaxation time constant, τ, defined as the time taken for the reaction force to decrease to 63% of its peak magnitude to the equilibrium magnitude, was approximately 36.1 s. This relaxation time was the same as that of the final step of the stress relaxation experiment (Bonifasi-Lista et al., 2005). This was achieved with a penalty parameter of $\kappa=1.55$. Since ligaments contain 65–75% water by weight, the fluid volume fraction was selected to be 0.7 (Benjamin and Ralphs, 1997). A second stress relaxation simulation was conducted by stretching the model to 3% strain over 1 s. The average fiber stress over all elements, average Poisson's ratio over all elements, and net fluid flux out of the material were plotted as functions of time. This simulation was repeated with the nearly incompressible material description assigned to the solid phase of the model and the time-dependent behavior of both models was compared. The mesh density of the cylinder used during this simulation was varied to confirm convergence. A converged mesh was defined by producing a change in the peak reaction force of less than 0.5% from the previous mesh.

2.4. Parameter sensitivity study

The penalty parameter κ, matrix coefficient μ, initial permeability k_0, and the cross sectional area of the cylinder represented by the quarter symmetry model were increased and decreased by 20% of their initial value used in the biphasic simulation. The sensitivity of the biphasic simulation to the above parameters was quantified by examining the change in the normalized reaction force at equilibrium of the final displacement step as well as the relaxation time constant, τ.

3. Results

3.1. Quasi-static simulation of uniaxial extension

The quasi-static uniaxial simulation revealed that the new model could predict comparable stress–strain behavior to the nearly incompressible model (Fig. 3-Top). While the nearly incompressible model predicted a Poisson's ratio that decreased slightly from 0.50 to about 0.48, the new ligament constitutive model predicted a Poisson's ratio that decreased from 5.79 to 2.57 as a function of applied strain (Fig. 3-Bottom).

3.2. Biphasic simulation of uniaxial stress relaxation

The biphasic simulation that used the new model to represent the solid phase predicted substantial stress relaxation. The stress predicted by this simulation peaked at 9.08 MPa and decreased to 4.08 MPa at equilibrium. This equilibrium value was consistent with the stress predicted by the one-element quasi-static simulation at 3% strain (Fig. 4A). The biphasic simulation that used the nearly incompressible model for the solid phase predicted a constant stress of 4.02 MPa with no relaxation. Simulations that represented the solid phase with the new model also predicted substantial fluid flux out of the material, peaking at 2.37×10^{-2} mm^3/s, while the nearly incompressible simulations predicted almost no fluid flux out of the material, peaking at 3.2×10^{-5} mm^3/s upon initial loading (Fig. 4B). The Poisson's ratio of the nearly incompressible simulations decreased slightly from

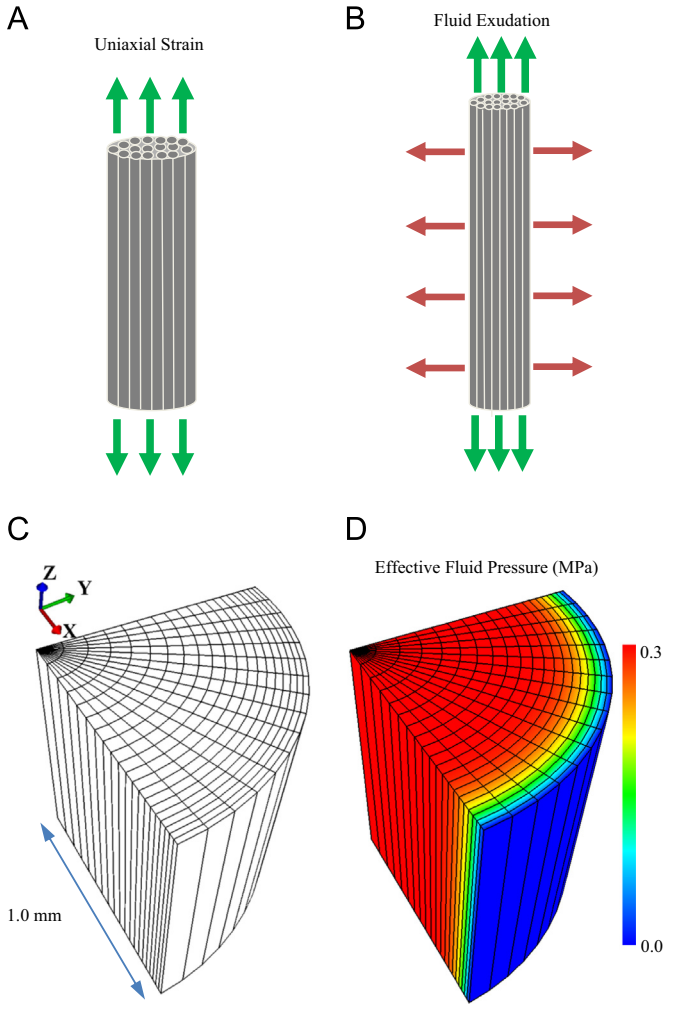

Fig. 2. Biphasic simulation of uniaxial stress relaxation. A and B: schematic of uniaxial extension and stress relaxation of a biphasic, transversely isotropic material with large Poisson's ratio. As uniaxial strain is applied (green arrows), the material will retract laterally and generate internal pressure. If the material has a finite permeability, this pressure will drive fluid exudation (red arrows). C: a quarter symmetry cylindrical finite element mesh was used in the biphasic simulations. The fiber direction is aligned with the *z*-axis. and the mesh was biased to place more elements toward the exterior surface to accurately predict the larger pressure gradient in this area. D. Effective fluid pressure at peak elongation before stress relaxation as predicted by finite element simulation. Pressure is highest at the center of the model and drops to zero at the free edge. (For interpretation of references to color in this figure legend, the reader is referred to the web version of this article.)

0.50 to 0.49, while the Poisson's ratio for the new model simulations increased from 0.68 upon initial loading to 4.01 at full relaxation. This was also the Poisson's ratio predicted by the quasi-static simulation at 3% strain (Fig. 4C).

3.3. *Parameter sensitivity study*

Decreasing the penalty parameter κ by 20% caused the normalized equilibrium reaction force to increase by 13.8% and the relaxation rate parameter τ to increase by 22.7%, while increasing it by 20% caused the normalized force to decrease by 10.8% and τ to decrease by 11.1%. Decreasing the initial permeability k_0 by 20% caused the normalized equilibrium reaction force to decrease by 0.9% and τ to increase by 24.9%, while increasing it by 20% caused the normalized force to increase by 0.8% and τ to decrease by 15.3%. Altering the matrix parameter μ by 20% in either direction had a negligible effect on both the normalized equilibrium force and relaxation rate. Decreasing the cylindrical radius by 20% caused the normalized equilibrium reaction force to increase by 2.75% and τ to decrease by 33.3%, while increasing it by 20% caused the normalized force to decrease by 1.4% and τ to increase by 40.0% (Fig. 5).

4. Discussion

This study demonstrated that the constitutive model can predict the large Poisson's ratios measured experimentally while still predicting a similar uniaxial stress–strain response as a nearly incompressible model describing uniaxial tension of human MCL. This new model was able to predict this large Poisson's ratio using a penalty based approach that could constrain the Poisson's ratio to follow any chosen function. Although micromechanical models that include explicit representation of microstructural features such as crimp and helical organization can predict large Poisson's ratios (Reese et al., 2010), the present approach is vastly less computationally expensive than micromechanical models, providing the potential for its use in large scale, whole joint models. The theoretical framework shows how any function could be implemented to describe the Poisson's ratio, by substituting the desired equation as a function of λ into Eq. (4) to derive another expression for the squared area ratio, which could then be incorporated into a similar strain energy equation. Thus, this method could be used for other applications where it is desirable to constrain the volumetric deformation of a material.

By representing the solid phase of a biphasic material with a realistic solid volume fraction and permeability, the model was able to predict time-dependent behavior that reflects observations for ligament and tendon. The lateral contraction caused by the large Poisson's ratio had the effect of forcing a substantial amount of fluid from the material. This is consistent with reports of fluid exudation from ligaments under uniaxial tension (Hannafin and Arnoczky, 1994; Helmer et al., 2006; Lanir et al., 1988; Wellen et al., 2004). Furthermore, the increased fluid pressure also led to an increase in fiber stress, which dissipates to the stress value predicted by the quasi-static simulation at equilibrium, resembling the characteristic stress relaxation curve of ligaments. Neither the large fluid flux nor the stress relaxation behavior were predicted when the nearly incompressible model was used for the solid phase. The Poisson's ratio of the new model also increased from a small value of 0.68 to the predicted value at 3% strain. The small initial Poisson's ratio suggests that when loading is initiated, the mixture behaves as nearly incompressible.

Similar behavior has been observed in the measurement of Poisson's ratio during stress relaxation of rat tail tendon fascicles (Reese and Weiss, 2013). The predictions are also consistent with those from a previous study (Buckley et al., 2013), where time-dependent lateral contraction during uniaxial tensile testing of mouse flexor carpi ulnaris tendon was influenced by changes in the ionic concentration of the surrounding fluid. Previous constitutive models that have been used to describe ligament and tendon stress relaxation behavior have explicitly included the time dependent response of the material in their constitutive models (Abramowitch and Woo, 2004; Lakes and Vanderby, 1999; Provenzano et al., 2002), and to date, none has attempted to describe the time dependent fluid motion or Poisson's ratio during relaxation.

The parameter sensitivity study demonstrated how the biphasic response of the model was altered by changes in material and biphasic parameters. The equilibrium reaction force was only sensitive to the penalty parameter κ, where increasing κ caused a decrease in the normalized equilibrium reaction force, indicating a larger peak force. This can be explained by understanding that

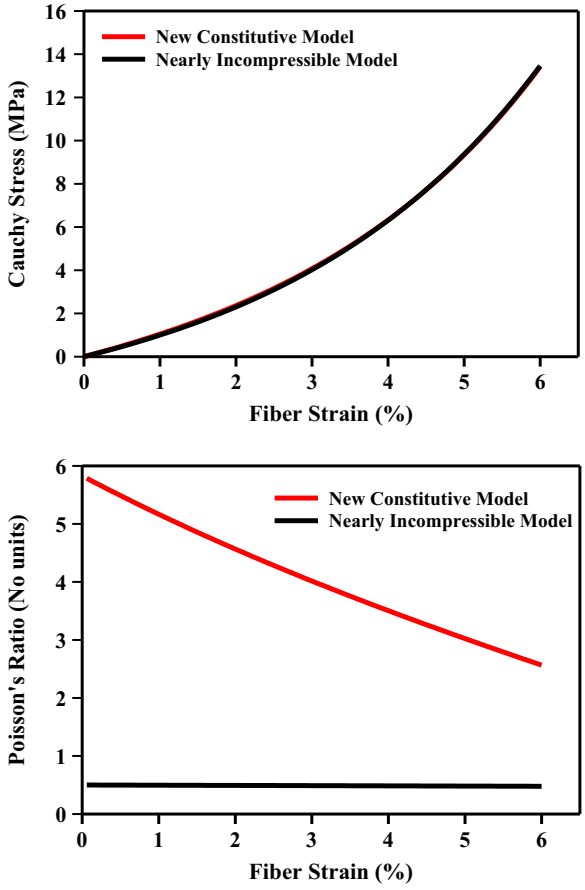

Fig. 3. Top – The new constitutive model was able to predict comparable stress–strain behavior to the previous model. Bottom – The new model predicted an apparent Poisson's ratio that decreased as a function of fiber stretch while the nearly incompressible model predicted a Poisson's ratio of about 0.5 that did not change substantially as a function of fiber strain.

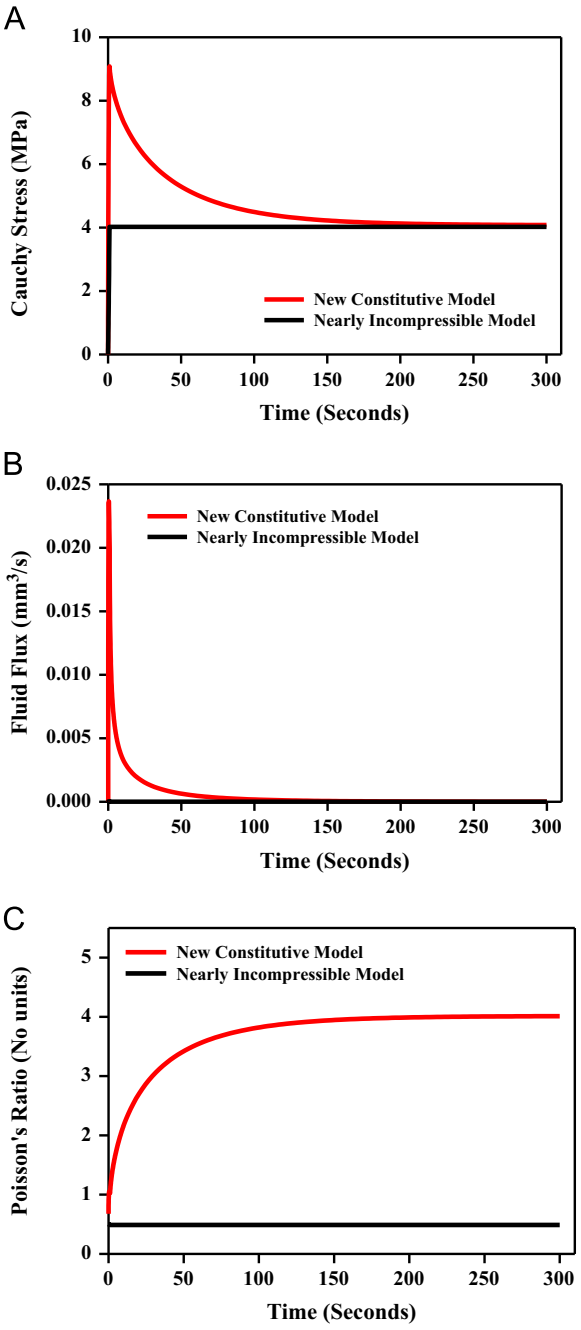

Fig. 4. A – The Cauchy stress as a function of time during the final displacement step of the biphasic simulation. The new model predicted substantial stress relaxation while the nearly incompressible model did not. B – Net fluid flux out of the surface of the cylinder during the final step of the biphasic simulation. The new model predicted a relatively large fluid flux while the nearly incompressible model predicted nearly no fluid flux. C – The Poisson's ratio during the final step of the biphasic simulation. The Poisson's ratio of the new model increased from a value of near 0.5 to the value predicted by the quasi-static simulation, while the nearly incompressible model predicted a Poisson's ratio of about 0.5.

increasing κ caused an increase in the lateral traction force in order to enforce the prescribed volumetric deformation, which in turn caused an increase in fluid pressure, leading to a larger peak force. The relaxation time constant τ was sensitive to κ, the initial permeability of the material, and the radius of the model. Again, increasing κ increased the lateral traction force, causing the model to contract more quickly, while increasing the permeability caused the fluid to exit the model more quickly, also allowing a faster relaxation. However, increasing the radius caused the model to relax more slowly, which is again expected since the fluid can only exude radially outward and increasing the distance that it must cross would increase the diffusive drag of the fluid. This behavior is predicted by biphasic theory and it has been shown by analytical calculations for unconfined compression of cartilage that an increase in radius causes a decrease in the relaxation rate (Armstrong et al., 1984; Cohen et al., 1998). Thus the effects of changes in the model parameters can be interpreted in terms of our expectations for the material behavior of a biphasic material with a large Poisson's ratio.

It is worth noting that κ can be interpreted in two different ways depending on the type of simulation under investigation. For the elastic case, κ behaves as a penalty parameter and serves to enforce the Poisson's ratio. In this case, there is an upper limit of κ that sufficiently enforces the volumetric constraint, and increasing the κ above this value has no further effect. For biphasic simulations, κ takes on a physical interpretation in which it determines the lateral traction force that drives volumetric contraction. Although the equilibrium value of Poisson's ratio is the same provided the value of κ is above the upper limit as determined by the elastic case, increasing κ past this value has the added effect of increasing the lateral traction force, causing faster relaxation and a larger peak reaction force. If boundary restraints prevent lateral contraction, κ will control the magnitude of the reaction force at the boundaries. Thus, for elastic simulations, it is only necessary to select κ to sufficiently enforce the desired Poisson's ratio. For biphasic simulations, κ must be determined based on time-dependent experimental data. Methods to decouple these two effects are potential areas for further investigation.

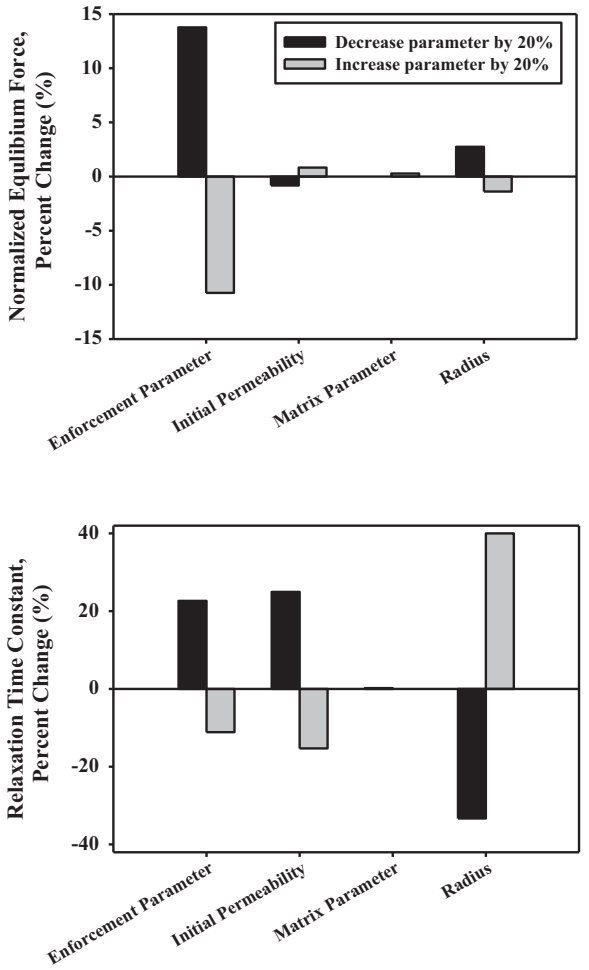

Fig. 5. Results of the parameter sensitivity study for the biphasic simulation. Left – Percent change of the normalized equilibrium reaction force predicted by the biphasic simulation upon increasing and decreasing each parameter by 20%. Right – Percent change of original relaxation parameter τ predicted by the biphasic simulation upon increasing and decreasing each parameter by 20%.

There are several limitations of the approach that merit discussion. First, the constitutive model was parameterized based solely on experimental measurements of uniaxial stress–strain behavior and Poisson's ratio. This was a reasonable approach given the goals of the analyses. Second, the matrix was modeled using a compressible neo-Hookean strain energy, which leads to a linear stress–strain relationship in shear or transverse to the fiber direction. The experimentally measured force response of ligament under shear along the fiber direction is more accurately described as exponential (Weiss et al., 2002). Since transverse loading was not the focus of the study, this was an appropriate simplification. A final limitation is that the data used to parameterize the Poisson's behavior of our model was taken from a relatively small range of longitudinal strain. Since there is limited data in the literature reporting the Poisson's ratio as a function of fiber stretch, especially at larger values, further experiments must be performed to obtain this data to ensure the model is valid for larger values of strain.

In single-element FE simulations of uniaxial extension at larger fiber strains, we observed that the volume ratio of the element began to increase after $\lambda=1.05$. Since the volume ratio under uniaxial tension is $J=\lambda\alpha^2$, we can use Eq. (7) for α as a function of λ to obtain an analytical expression for the volume ratio as a function of fiber stretch. This equation has a minimum at $\lambda=(1+2m-2v_0)/(2m)$, which for the parameters listed in Table 1, occurs at $\lambda=1.053$. The volume ratio is predicted to increase after this stretch ratio, as we observed. Although the increase in volume at higher values of fiber stretch does not reflect realistic volumetric behavior, it is a mathematical consequence of using a linear function to describe the Poisson's ratio. This observation emphasizes the need for experimental studies of the Poisson's ratio at higher values of axial strain, to guide the specification of a function that more accurately reflects realistic ligament volumetric behavior over the entire physiological range of axial strain.

Conflict of interest statement

None of the authors have any disclosures to make related to conflict of interest with other people or organizations that could inappropriately influence (bias) their work.

Acknowledgments

Support from NIH Grants #R01AR047369, #R01GM083925 and #R01EB015133 is gratefully acknowledged.

Appendix A. Cross sectional area derivation with the Cayley–Hamilton theorem and Nanson's relation.

Using Nanson's relation (Humphrey, 2002) and the Cayley–Hamilton theorem (Spencer, 1980), we can derive an alternate form of $(da/dA)^2$ as represented by Eq. (9) in terms of the transversely isotropic strain invariants as follows:

$$\begin{aligned} I_1 &= \mathrm{tr}(\mathbf{C}) \\ I_2 &= \tfrac{1}{2}\left((\mathrm{tr}(\mathbf{C}))^2 - \mathrm{tr}(\mathbf{C}^2)\right) \\ I_3 &= \det(\mathbf{C}) = J^2 \\ I_4 &= \mathbf{a}_0 \cdot \mathbf{C} \cdot \mathbf{a}_0 = \lambda^2 \\ I_5 &= \mathbf{a}_0 \cdot \mathbf{C}^2 \cdot \mathbf{a}_0. \end{aligned} \tag{A1}$$

The tensor $\mathbf{C}$ is the right Cauchy–Green deformation tensor, $\mathbf{C}=\mathbf{F}^{\mathrm{T}}\mathbf{F}$, where $\mathbf{F}$ is the deformation gradient and $J=\det(\mathbf{F})$ is the volume ratio. The variable λ is the stretch ratio along the direction of loading, $\mathbf{a}$ and $\mathbf{a}_0$ are the deformed and the reference fiber direction unit vectors, respectively, and da and dA are the deformed and the undeformed material cross sectional areas, respectively, normal to the direction of loading. Nanson's relation states that for a given area

$$\mathbf{a}\, da = J\mathbf{F}^{-\mathrm{T}} \cdot \mathbf{a}_0\, dA. \tag{A2}$$

The Cayley–Hamilton theorem states that for any tensor $\mathbf{A}$

$$\mathbf{A}^3 - I_1\mathbf{A}^2 + I_2\mathbf{A} - I_3\mathbf{1} = \mathbf{0}. \tag{A3}$$

By selecting the right Cauchy–Green deformation tensor $\mathbf{C}=\mathbf{F}^{\mathrm{T}}\mathbf{F}$ to replace the $\mathbf{A}$ tensor in (A3), we are left with

$$\mathbf{C}^3 - I_1\mathbf{C}^2 + I_2\mathbf{C} - I_3\mathbf{1} = \mathbf{0}. \tag{A4}$$

Rearranging Eq. (A4) and noting that $I_3 = J^2$

$$\mathbf{C}^3 - I_1\mathbf{C}^2 + I_2\mathbf{C} = J^2\mathbf{1}. \tag{A5}$$

Multiplying (A2) with $J\mathbf{F}^T$

$$J\mathbf{F}^{\mathrm{T}} \cdot \mathbf{a}\, da = (J^2\mathbf{1}) \cdot \mathbf{a}_0\, dA. \tag{A6}$$

By substituting (A5) into the right hand side of (A6), we obtain

$$J\mathbf{F}^{\mathrm{T}} \cdot \mathbf{a}\, da = (\mathbf{C}^3 - I_1\mathbf{C}^2 + I_2\mathbf{C}) \cdot \mathbf{a}_0\, dA. \tag{A7}$$

The initial fiber direction $\mathbf{a}_0$ transforms into the current configuration using the deformation gradient

$$\mathbf{F}\cdot\mathbf{a}_0=\lambda\mathbf{a}, \tag{A8}$$

which can be rearranged to show that

$$\mathbf{a}=\frac{1}{\lambda}\mathbf{F}\cdot\mathbf{a}_0.$$

We can use this equation to replace $\mathbf{a}$ in the left-hand side of (A7) to show that

$$\frac{J}{\lambda}\mathbf{F}^{\mathrm{T}}\mathbf{F}\cdot\mathbf{a}_0\,da=(\mathbf{C}^3-I_1\mathbf{C}^2+I_2\mathbf{C})\cdot\mathbf{a}_0\,dA, \tag{A9}$$

which can also be written as

$$\frac{J}{\lambda}\mathbf{C}\cdot\mathbf{a}_0\,da=(\mathbf{C}^3-I_1\mathbf{C}^2+I_2\mathbf{C})\cdot\mathbf{a}_0\,dA. \tag{A10}$$

Premultiplying both sides of (A10) by the 2nd order tensor $\mathbf{C}^{-1}$, and then taking the inner product of both sides of the resulting equation the vector $\mathbf{a}_0$ gives

$$\frac{J}{\lambda}\mathbf{a}_0\cdot\mathbf{C}^{-1}\mathbf{C}\cdot\mathbf{a}_0\,da=\mathbf{a}_0\cdot\mathbf{C}^{-1}(\mathbf{C}^3-I_1\mathbf{C}^2+I_2\mathbf{C})\cdot\mathbf{a}_0\,dA, \tag{A11}$$

which can also be written as

$$\frac{J}{\lambda}da=(\mathbf{a}_0\cdot\mathbf{C}^2\cdot\mathbf{a}_0-I_1\mathbf{a}_0\cdot\mathbf{C}\cdot\mathbf{a}_0+I_2\mathbf{a}_0\cdot\mathbf{a}_0)dA. \tag{A12}$$

We can simplify the terms on the right hand side into strain invariants based in (A1) and divide both sides by dA

$$\frac{J}{\lambda}\frac{da}{dA}=I_5-I_1I_4+I_2. \tag{A13}$$

Since, for a deformation of a cube of transversely isotropic material along the fiber direction the volume ratio of the deformation will be given by

$$J=\lambda\alpha^2, \tag{A14}$$

where α is the stretch ratio in the directions transverse to the direction of loading. For a representative cube of material, the change in cross sectional area transverse to the fiber direction is related by

$$\alpha^2=\frac{da}{dA}. \tag{A15}$$

Thus by rearranging (A14) and replacing J/λ in (A13)

$$\boxed{\left(\frac{da}{dA}\right)^2=I_5-I_1I_4+I_2.} \tag{A16}$$

Appendix B. Cauchy stress and spatial elasticity tensor derivation for a transversely isotropic compressible hyperelastic material.

In order to implement the strain energy equation presented in this paper in the finite element solver FEBio, the Cauchy stress tensor and spatial elasticity tensor must be calculated. The derivation of a general form for of both the Cauchy stress tensor and spatial elasticity tensors for a transversely isotropic compressible hyperelastic material is presented in this appendix.

For some strain energy equation W, the 2nd Piola–Kirchhoff stress $\mathbf{S}$ can be derived using the right Cauchy–Green deformation tensor $\mathbf{C}$

$$\mathbf{S}=2\frac{\partial W}{\partial\mathbf{C}}. \tag{A17}$$

If W is expressed in terms of the transversely isotropic strain invariants I_α, where α ranges from 1 to 5 as shown in (A1), using the chain rule, Eq. (A17) can be expressed as

$$\mathbf{S}=2\sum_{\alpha=1}^{5}\left(\frac{\partial W}{\partial I_\alpha}\frac{\partial I_\alpha}{\partial\mathbf{C}}\right). \tag{A18}$$

The derivatives $\partial I_\alpha/\partial\mathbf{C}$ for each of the transversely isotropic strain invariants are as follows:

$$\begin{aligned}
&\frac{\partial I_1}{\partial\mathbf{C}}=\mathbf{1}\\
&\frac{\partial I_2}{\partial\mathbf{C}}=I_1\mathbf{1}-\mathbf{C}\\
&\frac{\partial I_3}{\partial\mathbf{C}}=I_2\mathbf{1}-I_1\mathbf{C}+\mathbf{C}^2=I_3\mathbf{C}^{-1}\\
&\frac{\partial I_4}{\partial\mathbf{C}}=\mathbf{a}_0\otimes\mathbf{a}_0\\
&\frac{\partial I_5}{\partial\mathbf{C}}=\mathbf{a}_0\otimes\mathbf{C}\cdot\mathbf{a}_0+\mathbf{a}_0\cdot\mathbf{C}\otimes\mathbf{a}_0.
\end{aligned} \tag{A19}$$

The derivatives $\partial W/\partial I_\alpha$ are found based on the specific strain energy equation represented in terms of the invariants, and are henceforth represented as W_α. The 2nd Piola–Kirchhoff stress can thus be written

$$\begin{aligned}
\mathbf{S}=&W_1\mathbf{1}+W_2(I_1\mathbf{1}-\mathbf{C})+W_3(I_3\mathbf{C}^{-1})+W_4(\mathbf{a}_0\otimes\mathbf{a}_0)\\
&+W_5(\mathbf{a}_0\otimes\mathbf{C}\cdot\mathbf{a}_0+\mathbf{a}_0\cdot\mathbf{C}\otimes\mathbf{a}_0).
\end{aligned} \tag{A20}$$

The Cauchy stress can be found by transforming $\mathbf{S}$ into the current spatial configuration via a push forward operation

$$\boldsymbol{\sigma}=\varphi^*\,\mathbf{S}, \tag{A21}$$

where φ^* represents the push forward operator, which for some second order tensor $\mathbf{A}$ is

$$\varphi^*\mathbf{A}=\frac{1}{J}\mathbf{F}\mathbf{A}\mathbf{F}^{\mathrm{T}}. \tag{A22}$$

Only the tensors in (A20) are transformed by the push forward operation, while the invariants and the strain energy derivatives are constants and can thus be factored out of the transformation. The transformed tensors are as follows:

$$\begin{aligned}
&\varphi^*1=\tfrac{1}{J}\mathbf{F}\mathbf{1}\mathbf{F}^{\mathrm{T}}=\tfrac{1}{J}\mathbf{B}\\
&\varphi^*\mathbf{C}=\frac{1}{J}\mathbf{F}(\mathbf{F}^{\mathrm{T}}\mathbf{F})\mathbf{F}^{\mathrm{T}}=\frac{1}{J}\mathbf{B}^2\\
&\varphi^*\mathbf{C}^{-1}=\frac{1}{J}\mathbf{F}(\mathbf{F}^{\mathrm{T}}\mathbf{F})^{-1}\mathbf{F}^{\mathrm{T}}=\frac{1}{J}\mathbf{F}(\mathbf{F}^{-1}\mathbf{F}^{-\mathrm{T}})\mathbf{F}^{\mathrm{T}}=\frac{1}{J}\mathbf{1}\\
&\varphi^*(\mathbf{a}_0\otimes\mathbf{a}_0)=\frac{\lambda^2}{J}(\mathbf{a}\otimes\mathbf{a})=\frac{I_4}{J}(\mathbf{a}\otimes\mathbf{a})\\
&\varphi^*(\mathbf{a}_0\otimes\mathbf{C}\cdot\mathbf{a}_0)=\frac{I_4}{J}(\mathbf{a}\otimes\mathbf{a})\cdot\mathbf{B}\\
&\varphi^*(\mathbf{a}_0\cdot\mathbf{C}\otimes\mathbf{a}_0)=\frac{I_4}{J}\mathbf{B}\cdot(\mathbf{a}\otimes\mathbf{a}),
\end{aligned} \tag{A23}$$

where the left Cauchy–Green deformation tensor $\mathbf{B}=\mathbf{F}\mathbf{F}^{\mathrm{T}}$, and $\mathbf{a}$ is the fiber direction vector in the deformed configuration. The Cauchy stress $\boldsymbol{\sigma}$ can now be found by replacing transformed tensors as shown in (A23) into (A20)

$$\begin{aligned}
\boldsymbol{\sigma}=\frac{2}{J}\Big(&(W_1+I_1W_2)\mathbf{B}-W_2\mathbf{B}^2+W_3(I_3\mathbf{1})+W_4I_4(\mathbf{a}\otimes\mathbf{a})\\
&+W_5I_4(\mathbf{a}\otimes\mathbf{a}\cdot\mathbf{B}+\mathbf{B}\cdot\mathbf{a}\otimes\mathbf{a})\Big).
\end{aligned} \tag{A24}$$

The symmetric fourth order material elasticity tensor $\mathbf{C}$ of the strain energy equation W can be calculated from the strain energy equation or the 2nd Piola–Kirchhoff stress as follows:

$$\mathbb{C}=4\frac{\partial^2W}{\partial\mathbf{C}^2}=2\frac{\partial\mathbf{S}}{\partial\mathbf{C}}. \tag{A25}$$

Calculating this derivative from (A20) using the chain rule

$$\frac{1}{4}\mathbb{C} = \mathbf{1}\otimes\frac{\partial W_1}{\partial \mathbf{C}} + W_2\mathbf{1}\otimes\frac{\partial I_1}{\partial \mathbf{C}} + I_1\mathbf{1}\otimes\frac{\partial W_2}{\partial \mathbf{C}} - \mathbf{C}\otimes\frac{\partial W_2}{\partial \mathbf{C}} - W_2\frac{\partial \mathbf{C}}{\partial \mathbf{C}} + W_3\mathbf{C}^{-1}\otimes\frac{\partial I_3}{\partial \mathbf{C}} + I_3\mathbf{C}^{-1}\otimes\frac{\partial W_3}{\partial \mathbf{C}} + W_3 I_3\frac{\partial \mathbf{C}^{-1}}{\partial \mathbf{C}} + \mathbf{a}_0\otimes\mathbf{a}_0\otimes\frac{\partial W_4}{\partial \mathbf{C}} + \frac{\partial I_5}{\partial \mathbf{C}}\otimes\frac{\partial W_5}{\partial \mathbf{C}} + W_5\frac{\partial^2 I_5}{\partial \mathbf{C}^2}. \tag{A26}$$

In order to calculate the derivatives in (A13) the following notation is introduced. For symmetric second order tensors $\mathbf{A}$ and $\mathbf{B}$

$$(\mathbf{A}\otimes\mathbf{B})_{ijkl} = A_{ij}B_{kl}$$
$$(\mathbf{A}\underline{\otimes}\mathbf{B})_{ijkl} = \tfrac{1}{2}\left(A_{ik}B_{jl} + A_{il}B_{jk}\right). \tag{A27}$$

The derivatives with respect to $\mathbf{C}$ as noted in (A26) are as follows:

$$\frac{\partial \mathbf{C}}{\partial \mathbf{C}} = \mathbf{1}\underline{\otimes}\mathbf{1}$$
$$\frac{\partial \mathbf{C}^{-1}}{\partial \mathbf{C}} = -\mathbf{C}^{-1}\underline{\otimes}\mathbf{C}^{-1} \tag{A28}$$
$$\frac{\partial^2 I_5}{\partial \mathbf{C}^2} = \mathbf{1}\underline{\otimes}(\mathbf{a}_0\otimes\mathbf{a}_0) + (\mathbf{a}_0\otimes\mathbf{a}_0)\underline{\otimes}\mathbf{1},$$

and

$$\frac{\partial W_\alpha}{\partial \mathbf{C}} = \sum_{\alpha=1}^{5}\frac{\partial}{\partial \mathbf{C}}\left(\frac{\partial W}{\partial I_\alpha}\right) = \sum_{\alpha=1}^{5}\frac{\partial W_\alpha}{\partial I_\beta}\frac{\partial I_\beta}{\partial \mathbf{C}} = (W_{\alpha 1} + I_1 W_{\alpha 2})\mathbf{1} - W_{\alpha 2}\mathbf{C} + W_{\alpha 3}I_3\mathbf{C}^{-1} + W_{\alpha 4}(\mathbf{a}_0\otimes\mathbf{a}_0) + W_{\alpha 5}(\mathbf{a}_0\otimes\mathbf{C}\cdot\mathbf{a}_0 + \mathbf{a}_0\cdot\mathbf{C}\otimes\mathbf{a}_0). \tag{A29}$$

Note that the derivatives $W_{\alpha\beta}$ where α and β range from 1 to 5 are the second derivatives of the strain energy with respect to the corresponding strain invariants. Replacing the derivatives in (A26)

$$\begin{aligned}\frac{1}{4}\mathbb{C} = {} & (W_{11} + I_1 W_{12})(\mathbf{1}\otimes\mathbf{1}) - W_{12}(\mathbf{1}\otimes\mathbf{C}) + W_{13}I_3(\mathbf{1}\otimes\mathbf{C}^{-1}) \\ & + W_{14}(\mathbf{1}\otimes\mathbf{a}_0\otimes\mathbf{a}_0) + W_{15}(\mathbf{1}\otimes(\mathbf{a}_0\otimes\mathbf{C}\cdot\mathbf{a}_0 + \mathbf{a}_0\cdot\mathbf{C}\otimes\mathbf{a}_0)) + W_2(\mathbf{1}\otimes\mathbf{1}) \\ & + (I_1 W_{21} + I_1^2 W_{22})(\mathbf{1}\otimes\mathbf{1}) - I_1 W_{22}(\mathbf{1}\otimes\mathbf{C}) + I_1 I_3 W_{23}(\mathbf{1}\otimes\mathbf{C}^{-1}) \\ & + I_1 W_{24}(\mathbf{1}\otimes\mathbf{a}_0\otimes\mathbf{a}_0) + I_1 W_{25}(\mathbf{1}\otimes(\mathbf{a}_0\otimes\mathbf{C}\cdot\mathbf{a}_0 + \mathbf{a}_0\cdot\mathbf{C}\otimes\mathbf{a}_0)) \\ & - (W_{21} + I_1 W_{22})(\mathbf{C}\otimes\mathbf{1}) + W_{22}(\mathbf{C}\otimes\mathbf{C}) - I_3 W_{23}(\mathbf{C}\otimes\mathbf{C}^{-1}) \\ & - W_{24}(\mathbf{C}\otimes\mathbf{a}_0\otimes\mathbf{a}_0) - W_{25}(\mathbf{C}\otimes(\mathbf{a}_0\otimes\mathbf{C}\cdot\mathbf{a}_0 + \mathbf{a}_0\cdot\mathbf{C}\otimes\mathbf{a}_0)) \\ & - W_2\left(\mathbf{1}\underline{\otimes}\mathbf{1}\right) + I_3 W_3(\mathbf{C}^{-1}\otimes\mathbf{C}^{-1}) + (I_3 W_{31} + I_1 I_3 W_{32})(\mathbf{C}^{-1}\otimes\mathbf{1}) \\ & - I_3 W_{32}(\mathbf{C}^{-1}\otimes\mathbf{C}) + I_3^2 W_{33}(\mathbf{C}^{-1}\otimes\mathbf{C}^{-1}) + I_3 W_{34}(\mathbf{C}^{-1}\otimes\mathbf{a}_0\otimes\mathbf{a}_0) \\ & + I_3 W_{35}\left(\mathbf{C}^{-1}\otimes(\mathbf{a}_0\otimes\mathbf{C}\cdot\mathbf{a}_0 + \mathbf{a}_0\cdot\mathbf{C}\otimes\mathbf{a}_0)\right) - W_3 I_3\left(\mathbf{C}^{-1}\underline{\otimes}\mathbf{C}^{-1}\right) \\ & + (W_{41} + I_1 W_{42})(\mathbf{a}_0\otimes\mathbf{a}_0\otimes\mathbf{1}) - W_{42}(\mathbf{a}_0\otimes\mathbf{a}_0\otimes\mathbf{C}) \\ & + I_3 W_{43}(\mathbf{a}_0\otimes\mathbf{a}_0\otimes\mathbf{C}^{-1}) + W_{44}(\mathbf{a}_0\otimes\mathbf{a}_0\otimes\mathbf{a}_0\otimes\mathbf{a}_0) \\ & + W_{45}(\mathbf{a}_0\otimes\mathbf{a}_0\otimes(\mathbf{a}_0\otimes\mathbf{C}\cdot\mathbf{a}_0 + \mathbf{a}_0\cdot\mathbf{C}\otimes\mathbf{a}_0)) + (W_{51} + I_1 W_{52})\left(\frac{\partial I_5}{\partial \mathbf{C}}\otimes\mathbf{1}\right) \\ & - W_{52}\left(\frac{\partial I_5}{\partial \mathbf{C}}\otimes\mathbf{C}\right) + I_3 W_{53}\left(\frac{\partial I_5}{\partial \mathbf{C}}\otimes\mathbf{C}^{-1}\right) + W_{54}\left(\frac{\partial I_5}{\partial \mathbf{C}}\otimes\mathbf{a}_0\otimes\mathbf{a}_0\right) \\ & + W_{55}\left(\frac{\partial I_5}{\partial \mathbf{C}}\otimes(\mathbf{a}_0\otimes\mathbf{C}\cdot\mathbf{a}_0 + \mathbf{a}_0\cdot\mathbf{C}\otimes\mathbf{a}_0)\right) \\ & + W_5\left(\mathbf{1}\underline{\otimes}(\mathbf{a}_0\otimes\mathbf{a}_0) + (\mathbf{a}_0\otimes\mathbf{a}_0)\underline{\otimes}\mathbf{1}\right).\end{aligned} \tag{A30}$$

For ease of notation, $\partial I_5/\partial\mathbf{C}$ was left in its current form instead of the expanded form listed in (A19). Recognizing that $W_{ab}=W_{ba}$, we can group the strain energy derivatives in (A30) by their tensors

$$\begin{aligned}\frac{1}{4}\mathbb{C} = {} & (W_{11} + 2I_1 W_{12} + W_2 + I_1^2 W_{22})(\mathbf{1}\otimes\mathbf{1}) - (W_{12} \\ & + I_1 W_{22})(\mathbf{1}\otimes\mathbf{C} + \mathbf{C}\otimes\mathbf{1}) + W_{22}(\mathbf{C}\otimes\mathbf{C}) - W_2\left(\mathbf{1}\underline{\otimes}\mathbf{1}\right) \\ & + (I_3 W_{13} + I_1 I_3 W_{23})(\mathbf{1}\otimes\mathbf{C}^{-1} + \mathbf{C}^{-1}\otimes\mathbf{1}) - I_3 W_{23}(\mathbf{C}\otimes\mathbf{C}^{-1} \\ & + \mathbf{C}^{-1}\otimes\mathbf{C}) \\ & + (I_3 W_3 + I_3^2 W_{33})(\mathbf{C}^{-1}\otimes\mathbf{C}^{-1}) - W_3 I_3\left(\mathbf{C}^{-1}\underline{\otimes}\mathbf{C}^{-1}\right) \\ & + (W_{14} + I_1 W_{24})(\mathbf{1}\otimes\mathbf{a}_0\otimes\mathbf{a}_0 \\ & + \mathbf{a}_0\otimes\mathbf{a}_0\otimes\mathbf{1}) - W_{24}(\mathbf{C}\otimes\mathbf{a}_0\otimes\mathbf{a}_0 + \mathbf{a}_0\otimes\mathbf{a}_0\otimes\mathbf{C}) \\ & + I_3 W_{34}(\mathbf{C}^{-1}\otimes\mathbf{a}_0\otimes\mathbf{a}_0 + \mathbf{a}_0\otimes\mathbf{a}_0\otimes\mathbf{C}^{-1}) \\ & + (W_{15} \\ & + I_1 W_{25})\left(\mathbf{1}\otimes\frac{\partial I_5}{\partial \mathbf{C}} + \frac{\partial I_5}{\partial \mathbf{C}}\otimes\mathbf{1}\right) - W_{25}\left(\mathbf{C}\otimes\frac{\partial I_5}{\partial \mathbf{C}} + \frac{\partial I_5}{\partial \mathbf{C}}\otimes\mathbf{C}\right) \\ & + I_3 W_{35}\left(\mathbf{C}^{-1}\otimes\frac{\partial I_5}{\partial \mathbf{C}} + \frac{\partial I_5}{\partial \mathbf{C}}\otimes\mathbf{C}^{-1}\right) \\ & + W_{45}\left(\mathbf{a}_0\otimes\mathbf{a}_0\otimes\frac{\partial I_5}{\partial \mathbf{C}} + \frac{\partial I_5}{\partial \mathbf{C}}\otimes\mathbf{a}_0\otimes\mathbf{a}_0\right) \\ & + W_{44}(\mathbf{a}_0\otimes\mathbf{a}_0\otimes\mathbf{a}_0\otimes\mathbf{a}_0) + W_{55}\left(\frac{\partial I_5}{\partial \mathbf{C}}\otimes\frac{\partial I_5}{\partial \mathbf{C}}\right) \\ & + W_5\left(\mathbf{1}\underline{\otimes}(\mathbf{a}_0\otimes\mathbf{a}_0) + (\mathbf{a}_0\otimes\mathbf{a}_0)\underline{\otimes}\mathbf{1}\right).\end{aligned} \tag{A31}$$

The fourth order spatial elasticity tensor $\mathbb{c}$ can be found by the push forward of the material elasticity tensor $\mathbb{C}$

$$\mathbb{c} = \varphi^*\mathbb{C}. \tag{A32}$$

In addition to the push forwards of the second order tensors listed in (A23), the fourth order dyadic tensor operators listed in (A27) push forward as follows:

$$\varphi^*(\mathbf{A}\otimes\mathbf{B}) = (\varphi^*\mathbf{A})\otimes(\varphi^*\mathbf{B})$$
$$\varphi^*(\mathbf{A}\underline{\otimes}\mathbf{B}) = (\varphi^*\mathbf{A})\underline{\otimes}(\varphi^*\mathbf{B}). \tag{A33}$$

The final form of our spatial elasticity tensor is

$$\begin{aligned}\frac{J}{4}\mathbb{c} = {} & (W_{11} + 2I_1 W_{12} + W_2 + I_1^2 W_{22})(\mathbf{B}\otimes\mathbf{B}) \\ & - (W_{12} + I_1 W_{22})(\mathbf{B}\otimes\mathbf{B}^2 + \mathbf{B}^2\otimes\mathbf{B}) + W_{22}(\mathbf{B}^2\otimes\mathbf{B}^2) \\ & - W_2\mathbf{B}\underline{\otimes}\mathbf{B} + (I_3 W_{13} + I_1 I_3 W_{23})(\mathbf{B}\otimes\mathbf{1} + \mathbf{1}\otimes\mathbf{B}) \\ & - I_3 W_{23}(\mathbf{B}^2\otimes\mathbf{1} + \mathbf{1}\otimes\mathbf{B}^2) + (I_3 W_3 + I_3^2 W_{33})(\mathbf{1}\otimes\mathbf{1}) \\ & - W_3 I_3(\mathbf{1}\underline{\otimes}\mathbf{1}) + (I_4 W_{14} + I_1 I_4 W_{24})(\mathbf{B}\otimes\mathbf{a}\otimes\mathbf{a} + \mathbf{a}\otimes\mathbf{a}\otimes\mathbf{B}) \\ & - I_4 W_{24}(\mathbf{B}^2\otimes\mathbf{a}\otimes\mathbf{a} + \mathbf{a}\otimes\mathbf{a}\otimes\mathbf{B}^2) + I_3 I_4 W_{34}(\mathbf{1}\otimes\mathbf{a}\otimes\mathbf{a} + \mathbf{a}\otimes\mathbf{a}\otimes\mathbf{1}) \\ & + (I_4 W_{15} + I_1 I_4 W_{25})(\mathbf{B}\otimes(\mathbf{a}\otimes\mathbf{a}\cdot\mathbf{B} + \mathbf{B}\cdot\mathbf{a}\otimes\mathbf{a}) \\ & + (\mathbf{a}\otimes\mathbf{a}\cdot\mathbf{B} + \mathbf{B}\cdot\mathbf{a}\otimes\mathbf{a})\otimes\mathbf{B}) \\ & - W_{25}I_4\left(\mathbf{B}^2\otimes(\mathbf{a}\otimes\mathbf{a}\cdot\mathbf{B} + \mathbf{B}\cdot\mathbf{a}\otimes\mathbf{a}) + (\mathbf{a}\otimes\mathbf{a}\cdot\mathbf{B} + \mathbf{B}\cdot\mathbf{a}\otimes\mathbf{a})\otimes\mathbf{B}^2\right) \\ & + I_3 I_4 W_{35}(\mathbf{1}\otimes(\mathbf{a}\otimes\mathbf{a}\cdot\mathbf{B} + \mathbf{B}\cdot\mathbf{a}\otimes\mathbf{a}) + (\mathbf{a}\otimes\mathbf{a}\cdot\mathbf{B} + \mathbf{B}\cdot\mathbf{a}\otimes\mathbf{a})\otimes\mathbf{1}) \\ & + W_{45}I_4{}^2(\mathbf{a}\otimes\mathbf{a}\otimes(\mathbf{a}\otimes\mathbf{a}\cdot\mathbf{B} + \mathbf{B}\cdot\mathbf{a}\otimes\mathbf{a}) + (\mathbf{a}\otimes\mathbf{a}\cdot\mathbf{B} + \mathbf{B}\cdot\mathbf{a}\otimes\mathbf{a})\otimes\mathbf{a}\otimes\mathbf{a}) \\ & + I_4{}^2 W_{44}(\mathbf{a}\otimes\mathbf{a}\otimes\mathbf{a}\otimes\mathbf{a}) \\ & + I_4^2 W_{55}((\mathbf{a}\otimes\mathbf{a}\cdot\mathbf{B} + \mathbf{B}\cdot\mathbf{a}\otimes\mathbf{a})\otimes(\mathbf{a}\otimes\mathbf{a}\cdot\mathbf{B} + \mathbf{B}\cdot\mathbf{a}\otimes\mathbf{a})) \\ & + I_4 W_5(\mathbf{B}\underline{\otimes}(\mathbf{a}\otimes\mathbf{a}) + (\mathbf{a}\otimes\mathbf{a})\underline{\otimes}\mathbf{B}).\end{aligned} \tag{A34}$$

Note that this document presents the general form of the Cauchy stress and spatial elasticity tensors for compressible, hyperelastic transversely isotropic materials. The first and second strain energy derivatives are specific to the strain energy function.

Due to their length, the strain energy derivatives specific to our combined strain energy function are not presented explicitly in this document and can be instead found in a Mathematical file in Supplementary File B.

Appendix C. Supplementary materials

Supplementary data associated with this article can be found in the online version at http://dx.doi.org/10.1016/j.jbiomech.2014.05.011.

References

Abramowitch, S.D., Woo, S.L., 2004. An improved method to analyze the stress relaxation of ligaments following a finite ramp time based on the quasi-linear viscoelastic theory. J. Biomech. Eng. 126, 92–97.

Armstrong, C.G., Lai, W.M., Mow, V.C., 1984. An analysis of the unconfined compression of articular cartilage. J. Biomech. Eng. 106, 165–173.

Beatty, M.F., Stalnaker, D.O., 1986. The Poisson function of finite elasticity. J. Appl. Mech. 53, 807–813.

Benjamin, M., Ralphs, J.R., 1997. Tendons and ligaments—an overview. Histol. Histopathol. 12, 1135–1144.

Bonet, J., Wood, R., 1997. Nonlinear Continuum Mechanics for Finite Element Analysis. Cambridge University Press, Cambridge, England.

Bonifasi-Lista, C., Lake, S.P., Small, M.S., Weiss, J.A., 2005. Viscoelastic properties of the human medial collateral ligament under longitudinal, transverse and shear loading. J. Orthop. Res. 23, 67–76.

Buckley, M.R., Sarver, J.J., Freedman, B.R., Soslowsky, L.J., 2013. The dynamics of collagen uncrimping and lateral contraction in tendon and the effect of ionic concentration. J. Biomech. 46, 2242–2249.

Butler, S.L., Kohles, S.S., Thielke, R.J., Chen, C., Vanderby Jr., R., 1997. Interstitial fluid flow in tendons or ligaments: a porous medium finite element simulation. Med. Biol. Eng. Comput. 35, 742–746.

Chen, C.T., Malkus, D.S., Vanderby Jr., R., 1998. A fiber matrix model for interstitial fluid flow and permeability in ligaments and tendons. Biorheology 35, 103–118.

Cohen, B., Lai, W.M., Mow, V.C., 1998. A transversely isotropic biphasic model for unconfined compression of growth plate and chondroepiphysis. J. Biomech. Eng. 120, 491–496.

Guerin, H.L., Elliott, D.M., 2007. Quantifying the contributions of structure to annulus fibrosus mechanical function using a nonlinear, anisotropic, hyperelastic model. J. Orthop. Res.: Off. Publ. Orthop. Res. Soc. 25, 508–516.

Hannafin, J.A., Arnoczky, S.P., 1994. Effect of cyclic and static tensile loading on water content and solute diffusion in canine flexor tendons: an in vitro study. J. Orthop. Res. 12, 350–356.

Helmer, K.G., Nair, G., Cannella, M., Grigg, P., 2006. Water movement in tendon in response to a repeated static tensile load using one-dimensional magnetic resonance imaging. J. Biomech. Eng. 128, 733–741.

Hewitt, J., Guilak, F., Glisson, R., Vail, T.P., 2001. Regional material properties of the human hip joint capsule ligaments. J. Orthop. Res. 19, 359–364.

Hirokawa, S., Tsuruno, R., 2000. Three-dimensional deformation and stress distribution in an analytical/computational model of the anterior cruciate ligament. J. Biomech. 33, 1069–1077.

Holmes, M.H., Mow, V.C., 1990. The nonlinear characteristics of soft gels and hydrated connective tissues in ultrafiltration. J. Biomech. 23, 1145–1156.

Humphrey, J.D., 2002. Cardiovascular Solid Mechanics: Cells, Tissues, and Organs, vol. xvi. Springer, New York p. 757.

Lakes, R.S., Vanderby, R., 1999. Interrelation of creep and relaxation: a modeling approach for ligaments. J. Biomech. Eng. 121, 612–615.

Lanir, Y., Salant, E.L., Foux, A., 1988. Physico-chemical and microstructural changes in collagen fiber bundles following stretch in-vitro. Biorheology 25, 591–603.

Lavagnino, M., Arnoczky, S.P., Kepich, E., Caballero, O., Haut, R.C., 2008. A finite element model predicts the mechanotransduction response of tendon cells to cyclic tensile loading. Biomech. Model. Mechanobiol. 7, 405–416.

Lynch, H.A., Johannessen, W., Wu, J.P., Jawa, A., Elliott, D.M., 2003. Effect of fiber orientation and strain rate on the nonlinear uniaxial tensile material properties of tendon. J. Biomech. Eng. 125, 726–731.

Maas, S.A., Ellis, B.J., Ateshian, G.A., Weiss, J.A., 2012. FEBio: finite elements for biomechanics. J. Biomech. Eng. 134, 011005.

Pioletti, D.P., Rakotomanana, L.R., Benvenuti, J.F., Leyvraz, P.F., 1998. Viscoelastic constitutive law in large deformations: applications to human knee ligaments and tendons. J. Biomech. 31, 753–757.

Provenzano, P.P., Lakes, R.S., Corr, D.T., Vanderby Jr., R., 2002. Application of nonlinear viscoelastic models to describe ligament behavior. Biomech. Model. Mechanobiol. 1, 45–57.

Purohit, P.K., Litvinov, R.I., Brown, A.E., Discher, D.E., Weisel, J.W., 2011. Protein unfolding accounts for the unusual mechanical behavior of fibrin networks. Acta Biomater. 7, 2374–2383.

Quapp, K.M., Weiss, J.A., 1998. Material characterization of human medial collateral ligament. J. Biomech. Eng. 120, 757–763.

Reese, S.P., Ellis, B.J., Weiss, J.A., 2013. Micromechanical model of a surrogate for collagenous soft tissues: development, validation and analysis of mesoscale size effects. Biomech. Model. Mechanobiol. 12, 1195–1204.

Reese, S.P., Maas, S.A., Weiss, J.A., 2010. Micromechanical models of helical superstructures in ligament and tendon fibers predict large Poisson's ratios. J. Biomech. 43, 1394–1400.

Reese, S.P., Weiss, J.A., 2013. Tendon fascicles exhibit a linear correlation between Poisson's ratio and force during uniaxial stress relaxation. J. Biomech. Eng. 135, 34501.

Screen, H.R.C., Cheng, V.W.T., 2007. The micro-structural strain response of tendon. J. Mater. Sci., 1–2.

Song, Y., Debski, R.E., Musahl, V., Thomas, M., Woo, S.L., 2004. A three-dimensional finite element model of the human anterior cruciate ligament: a computational analysis with experimental validation. J. Biomech. 37, 383–390.

Spencer, A.J.M., 1980. Continuum Mechanics. Longman, London; New York p. 183.

Urschel, J.D., Scott, P.G., Williams, H.T., 1988. The effect of mechanical stress on soft and hard tissue repair; a review. Br. J. Plast. Surg. 41, 182–186.

Weiss, J.A., France, E.P., Bagley, A.M., Blomstrom, G., 1992. Measurement of 2-D strains in ligaments under uniaxial tension. Transactions of 38th Annual Meeting of Orthopaedic Research Society, vol. 17, pp. 662.

Weiss, J.A., Gardiner, J.C., 2001. Computational modeling of ligament mechanics. Crit. Rev. Biomed. Eng. 29, 303–371.

Weiss, J.A., Gardiner, J.C., Bonifasi-Lista, C., 2002. Ligament material behavior is nonlinear, viscoelastic and rate-independent under shear loading. J. Biomech. 35, 943–950.

Weiss, J.A., Maakestad, B.J., 2006. Permeability of human medial collateral ligament in compression transverse to the collagen fiber direction. J. Biomech. 39, 276–283.

Wellen, J., Helmer, K.G., Grigg, P., Sotak, C.H., 2004. Application of porous-media theory to the investigation of water ADC changes in rabbit Achilles tendon caused by tensile loading. J. Magn. Reson. 170, 49–55.